Article

Biodegradable Poly(Butylene Succinate) Nanocomposites Based on Dimeric Surfactant Organomodified Clays with Enhanced Water Vapor Barrier and Mechanical Properties

Khadidja Taleb, Salima Saidi-Besbes,* Isabelle Pillin, and Yves Grohens

Read Online

ACCESS | 📊 Metrics & More | 📖 Article Recommendations | 🗎 Supporting Information

ABSTRACT: Biocomposites based on biodegradable polybutylene succinate (PBS) and organomodified clays (OMt) were prepared by melt blending process. The OMt nanofillers were obtained by ion exchange reaction between sodium montmorillonite (Mt) and gemini surfactants bearing 4-decyloxyphenylacetamide hydrophobic chains and ethylene or hexylene spacer. X-ray diffraction (XRD), scanning electron microscopy (SEM), transmission electron microscopy (TEM), and rheological measurement results showed that the investigated hybrids present a uniform dispersion with an exfoliation of clay into the PBS matrix, particularly for short spacer surfactant based composites. The effect of organoclay loading and composition on the thermal, mechanical, and barrier properties was also investigated. High clay loading and long gemini surfactant spacer lead to substantial improvement of Young modulus values by 21%, while low clay content induces a reduction of the hybrid's crystallinity due to strong OMt−PBS interactions. Compared to that of the neat PBS film, a significant reduction of the water vapor permeability (WVP) by 28% was obtained by adding only 3 wt % of PBS/OMt (2) which opens up prospects for this material in the field of food packaging. This study shows that gemini surfactant-modified organoclays can be used as effective nanofillers in a PBS matrix to access to value-added nanocomposites.
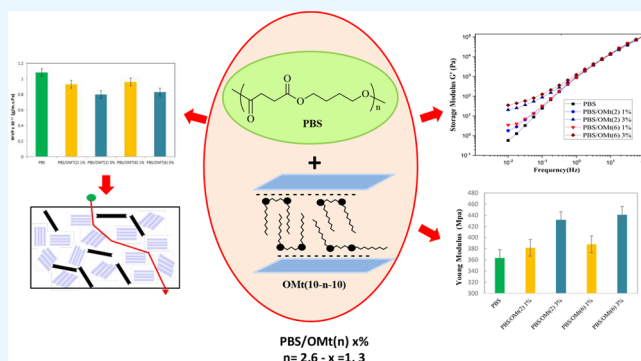
1. INTRODUCTION

Nowadays, biobased and synthetic biodegradable polymers are attracting increasing attention in green and sustainable economy as ecofriendly alternatives to petroleum-based traditional plastics. Aliphatic biodegradable polyesters are one of the most important classes that have been explored in several fields such as agriculture,[1] packaging,[2] biomedical, and pharmaceutical applications.[3] Among them, polybutylene succinate (PBS) has shown a great potential due to its favorable properties, similar to the widely used LDPE and PP, as thermal and chemical resistance, good processability, and flexibility.[4,5] However, some of PBS properties, such as water and gas barrier properties, softness, melt stability, and hydrolysis resistance, are still limited and insufficient for wider end-use applications.[5] For instance, in food packaging application, the enhancement of polymer's gas barrier properties is crucial for maintaining the quality of packaged foods. The main approaches used to prepare PBS polymer and related polymer blends with improved mechanical, thermal, and barrier properties consist of using multilayer films and/or binding the polymer matrix with nanofillers.[6] The latter method has been found to be more convenient and cost-effective. Several nanofillers have been tested for this purpose, including carbon nanotubes,[7] graphene,[8] nickel oxide,

quantum dots,[9] silica,[10] layered double hydroxide (LDH),[11] and clays.[12]

Clays are the most frequently used nanofillers for the preparation of polymer-based nanocomposites with enhanced properties. Besides being nontoxic, naturally available and inexpensive, their unique lamellar structure and high surface-to-volume ratio enable the improvement of the polymer's mechanical, thermal, and barrier properties even at low clay content (usually ≤5 wt %).[13] These benefits could be achieved through a good and uniform dispersion of the clay particles within the polymer matrix. Most of clay minerals are hydrophilic and thereby incompatibles with organic polymers. The main method to overcome this issue consists of the organomodification of clay by an ion exchange reaction of the structural clay cations with organic cations, such as organic cationic surfactants and polymers.
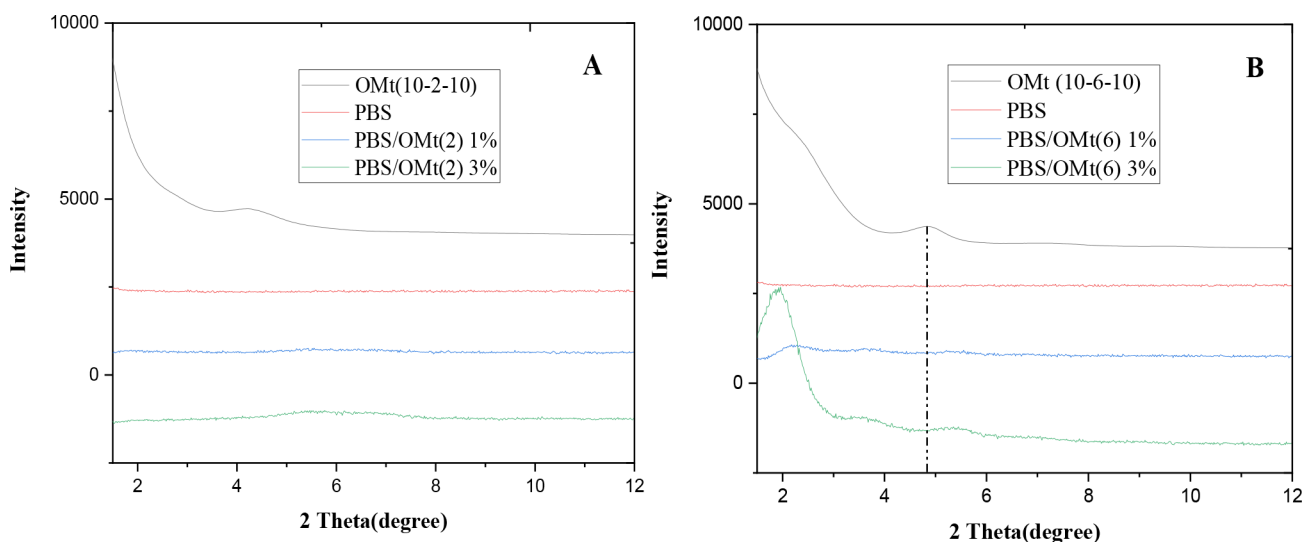
Figure 1. XRD patterns of neat PBS, OMts, and prepared nanocomposites based on (A) OMt (10−2−10) and (B) OMt (10−6−10) with 1 and 3 wt % clay loading.

For instance, Shih et al. studied the effect of surfactant structure on polybutylene succinate composites prepared by solution blending method with cetylpyridinium chloride (CPC) and cetyltrimethylammonium bromide (CTAB) organomodified "Kunipia F" montmorillionite (OMt). The thermal properties and particularly PBS glass transition temperature was obviously elevated by the addition of CPC-OMt compared with composites based on CTAB-OMt due to the steric constraint generated by the aromatic group. At the opposite, PBS/CTAB-OMt composites displayed higher storage and loss moduli than CPC based composites suggesting better interactions between CTAB aliphatic chains and PBS matrix.[14]

Ilsouk et al. elaborated a series of PBS nanocomposites with various loadings of CTAB-modified beidellite clay by situ polycondensation reaction between 1,4-butanediol and succinic anhydride. Compared to pure PBS, these hybrids showed a significant reduced water vapor permeability (WVP) and improved thermal stability.[5] Similar results have been reported for PBS nanocomposites prepared from OMt nanofillers containing different content of trihexyltetradecylphosphonium (0.4−1.2 times CEC of Mt). An ideal balance between thermal and mechanical properties was achieved at a surfactant quantity equivalent to 0.6 times the CEC.[15]

Recently, Karakehya et al. investigated the effect of hexadecyltrimethylammonium bromide modified clay (OMt), nanocrystalline cellulose (NCC), and carbon nanofiber (CNF) reinforcements on the mechanical, thermal, and surface properties of PBS nanocomposites. Among the studied nanocomposites, PBS-OMt showed the highest hydrophobicity and the best mechanical properties as well as a significant increase in hardness and modulus.[16]

Herein, we report engineered polymer nanocomposites based on polybutylene succinate (PBS) matrix reinforced with gemini surfactant-organomodified clays. Despite the outstanding surface properties of gemini surfactants and their efficiency for the compatibilization of organoclays in organic polymer,[17] to our knowledge, this is the first report on the application of gemini surfactant-treated clays as nanofillers in PBS matrix. Two organoclays based on gemini surfactant bearing different spacer lengths have been used for the

preparation of PBS nanocomposites by melt mixing process using a bivis extruder. The effect of OMt loading and surfactant structure on the morphology and mechanical, rheological, thermal, and vapor barrier properties of PBS nanocomposites will be evaluated and discussed.

2. RESULTS AND DISCUSSION

2.1. X-ray Diffraction. WAXD patterns of neat PBS, OMt (10−2−10) and OMt (10−6−10) organoclays and the related nanocomposites with different clay loading are shown in Figure 1. WAXD was used to probe the state of organoclay dispersion in the PBS matrix and the structure of polymer nanocomposites.

Two main diffraction picks were observed for both investigated OMts with an intense reflection at 2θ values of 4.19 and 4.83° corresponding to d_{001}-spacing values of 19.3 and 18.3 Å for OMt (10−2−10) and OMt (10−6−10), respectively. A shoulder was obtained at 2θ = 2.88 and 2.77° attributed to basal spacing of 36.9 and 36.7 Å, respectively.[18] The absence of the diffraction peak of pristine Na-Montmorillonite at lower d-spacing values (d_{001} = 11.2 Å) in the organoclay's XRD patterns and the expansion of the clay interlayer space indicate the successful intercalation of gemini surfactants. The occurrence of two-layer structure populations may be due to different arrangements of surfactant molecules within Mt interlayer space.[19]

None of OMt (10−2−10) characteristic basal reflections were observed in the XRD patterns of the PBS/OMt (2) 1% and PBS/OMt (2) 3% nanocomposites suggesting the formation of exfoliated structures as a result of an homogeneous and fine dispersion of organoclay into the polymer matrix.

An optimal interaction between PBS and clay surface during the melt blending mixing is of paramount importance to achieve such good clay dispersion. Indeed, this feature impacts substantially both the intercalation stage, where the polymer chains diffuse within OMt interlayer space, and the exfoliation stage to achieve the delamination of individual platelets and their diffusion into the melt.[20] We expect that the gemini surfactants will participate actively to these compatibilization process of clay with polymer organic matrix through the

establishment of hydrogen-bonding interactions between the amide functions of surfactant molecules and the carbonyl groups of PBS (Figure S1).

The nanocomposites prepared from organoclay containing longer spacer gemini surfactant OMt (10−6−10) showed a distinct behavior as depicted in Figure 1B. Two peaks were observed for PBS/OMt (6) 3% at 2θ values of 1.90 and 3.56° corresponding to a basal distance of 46.50 and 24.8 Å, respectively. The significant increase of the basal spacing values compared to the related OMts suggests the intercalation of the polymer chains into the clay galleries but with the retention of an ordered structure after melt extrusion.

An additional weak diffraction peak was also noticed at 2θ = 5.44° corresponding to d-spacing of 16.24 Å, lower than that recorded for OMt (10−6−10). This smaller d-spacing population can be attributed to a partial expulsion of surfactant molecules from the clay due to the thermomechanical stress applied during the melt mixing and/or to the crystallization of PBS during hybrids preparation resulting in the aggregation of some portion of clays.

Much less intense similar peaks were obtained for PBS/OMt(6)1% at 2θ values of 2.17° and 3.60° probably due to the lower clay content in this hybrid and/or to the formation of a mixture of intercalated/exfoliated morphologies.

The results indicate clearly that short spacer surfactant-based organoclay OMt (10−2−10) is more conducive for the preparation of exfoliated PBS/OMt hybrids probably due to higher compatibility with PBS matrix.

2.2. Rheology. The determination of rheological properties of nanocomposite materials in the molten state is essential to gain insight into their processability by means of extrusion and injection molding. It also provides complementary information about the dispersion state of organoclays within the polymer matrix. The logarithmic plot of storage modulus (G'), loss modulus (G''), and complex viscosity (η^*) of neat PBS and its related OMt-reinforced PBS hybrids containing 1 and 3 wt % of organoclays as functions of frequency were conducted in the linear viscoelastic region as shown in Figure 2A, 2B, and 2C, respectively.

The introduction of 1 wt % of organoclay induces a slight increase of storage modulus values as compared to pristine PBS but with the retention of the viscoelastic properties of PBS matrix (Figure 2A). This trend indicates that the nanocomposites exhibit a typical liquid-like behavior with fully relaxed PBS chains. Nevertheless, G' values become less frequency dependent in the terminal zone and start to develop a plateau particularly for high nanoclay content, thus suggesting a transition from the liquid-like viscoelastic behavior to solid-like one.[21] Such result might be due to the formation of a percolation network between the clay platelets in the PBS matrix.

Loss modulus (G'') of PBS/OMt nanocomposites evolved similarly as a function of frequency as shown in Figure 2B. The hybrids exhibit higher G'' values than PBS polymer on the whole studied frequency range that increase for higher frequencies and clay loading.

Likewise, the complex viscosity (η^*) curves (Figure 2C), based on linear dynamic oscillatory shear measurements, showed significant increase of η^* values for PBS nanocomposites particularly upon increasing the nanoclay content. This increment could be the result of a uniform nanodispersion of clay platelets within PBS matrix and the formation of structural network that hinders the movement
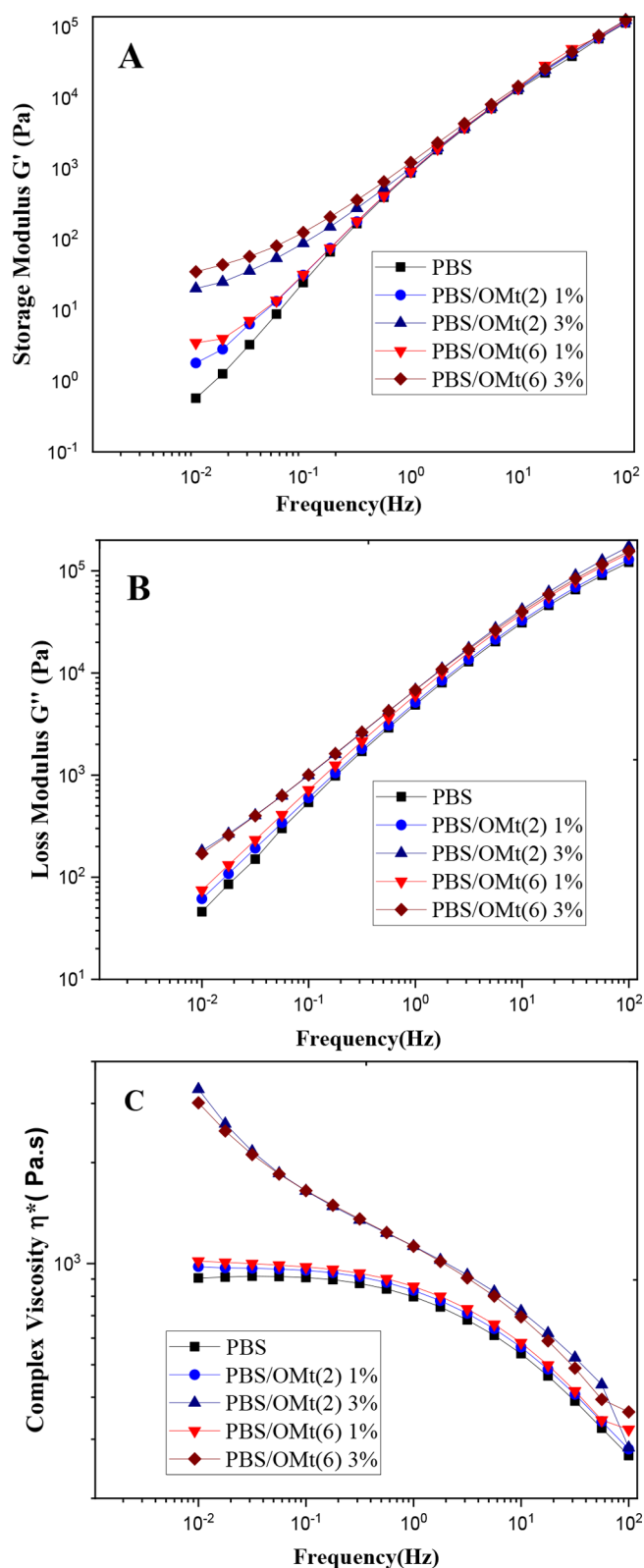

Figure 2. (A) Storage modulus (G'), (B) loss modulus (G''), and (C) complex viscosities (η^*) as a function of frequency for pristine PBS, PBS/OMt (2), and PBS/OMt (6) hybrids.

of PBS chains in the molten condition even at very low clay contents.[22]

It is worth noting that the observed Newtonian plateau at mid and low frequency ranges for PBS/OMt (n) 1%

nanocomposites disappeared in nanocomposites with 3 wt % clay content. The viscosity increases gradually with decreasing frequency for these hybrids indicating a pseudo solid-like response. This behavior reflects the good distribution of clay platelets within the PBS matrix. Such high compatibility could be attributed to the establishment of strong interfacial attractive interactions between organoclay and polymer matrix assured by Gemini surfactant molecules, as argued previously. Nevertheless, the impact of surfactant structure (i.e., the spacer length) on the viscoelastic properties of investigated nanocomposites remains less obvious.

2.3. Scanning Electron Microscopy (SEM). The morphology of the nanocomposites and the extent degree of nanoclays dispersion into PBS matrix was examined by scanning electron microscope. SEM micrographs of the cryo-fractured cross-section surfaces of neat PBS and its nanocomposites are shown in Figure 3.
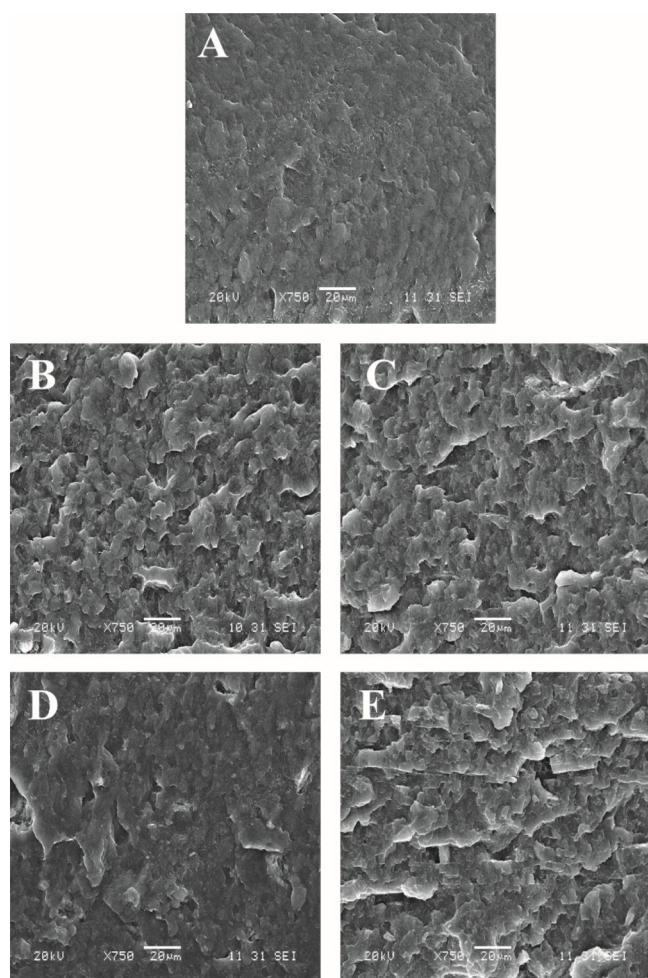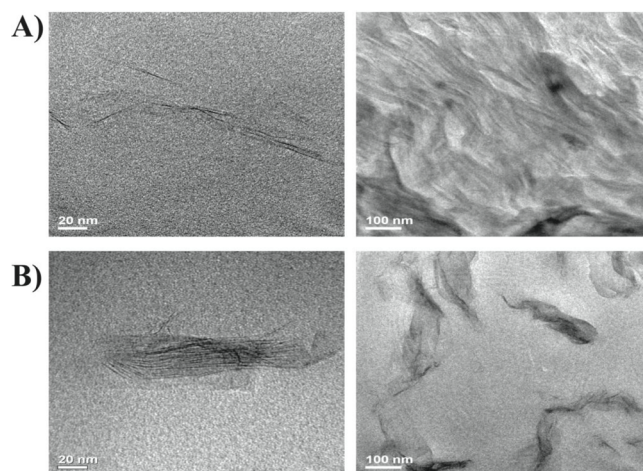

Figure 3. SEM images of (A) PBS, (B) PBS/OMt (2) 1%, (C) PBS/OMt (2) 3%, (D) PBS/OMt (6) 1%, and (E) PBS/OMt (6) 3% under a magnification of 750×.

Compared to the PBS sample that exhibits smooth surface, the nanocomposites showed a homogeneous dispersion of nanofillers in PBS matrix without evident formation of agglomerates, suggesting a good affinity between clays particles and PBS matrix. SEM images reveal also that the surface morphology of investigated hybrids is substantially affected by the nanofiller content and surfactant structure.

An obvious change in the morphology with an increase of the microvoids was evidenced in nanocomposite samples with respect to PBS matrix, and this all the more so for high clay content nanocomposites and short spacer surfactant-based OMt. Such microvoids play an important role in improving ductility and fracture toughness properties of the hybrid materials since they participate in energy absorption mechanism and induce better plastic deformation.[23]

2.4. Transmission Electron Microscopy (TEM). TEM analyses were carried out to further investigate the dispersion state of clay platelets in the internal structure of the composites at the nanometer scale. TEM images of PBS/OMt (2) 3% and PBS/OMt (6) 3% hybrids are presented in Figure 4. The dark entities represent the silicate layers intersection, while the brighter parts correspond to the polymer matrix.

Figure 4. TEM images of (A) PBS/OMt (2) 3% and (B) PBS/OMt (6) 3%.

PBS/OMt (2) 3% hybrid shows individualized exfoliated clay platelets which are homogeneously dispersed within the polymer matrix. The increase of the contact surface between clay platelets and PBS reflects the high affinity and compatibility between these two entities. Such good distribution and exfoliation should affect positively the mechanical and barriers properties of the corresponding hybrid. On the other hand, intercalated clay platelets dispersed as tactoids of limited size were highlighted in TEM images of PBS/OMt (6) 3% (Figure 4B). It, therefore, seems that TEM results are in good agreement with previously discussed XRD data.

2.5. Thermal Behavior. The effect of the addition of organoclays on the thermal stability of PBS nanocomposites was studied by TGA under nitrogen atmosphere. The TGA and DTG curves of PBS and its nanocomposites are presented in Figure 5. The thermal stability of hybrids was evaluated by the determination of the decomposition temperatures at 5, 10, 25, 50, and 75% weight loss and the maximum decomposition temperature (T_{max}). All investigated samples showed similar thermal degradation profile with a single degradation stage. The thermal degradation process seems to follows a one-step mechanism that can be related to the structural degradation of PBS matrix. The maximum degradation temperatures range from 402 to 408 °C indicating an excellent thermal stability (Table 1).
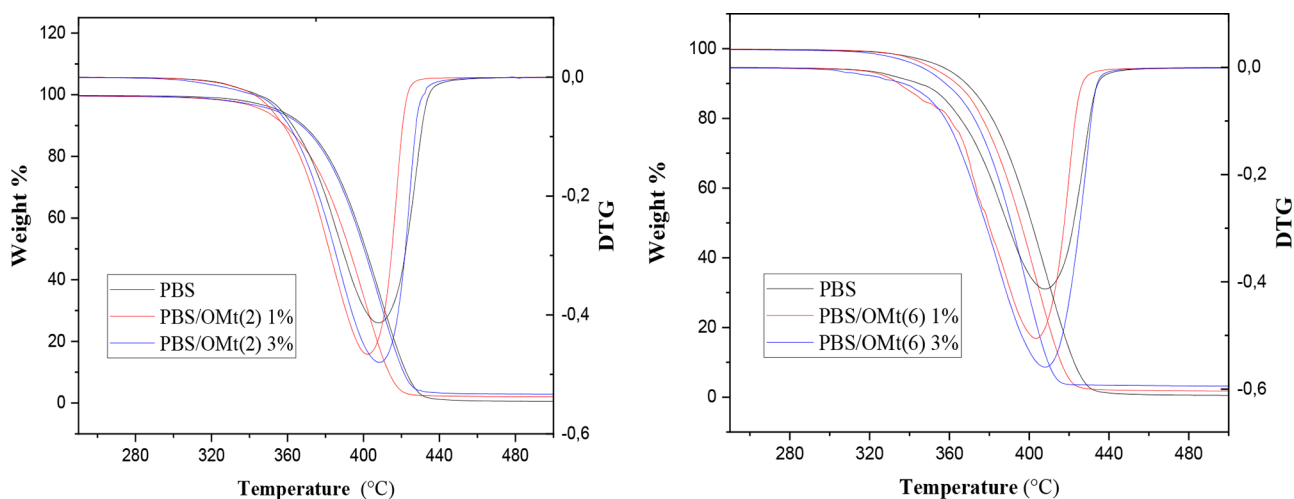
Figure 5. TG and DTG curves for PBS and PBS/OMt nanocomposites.

Table 1. Decomposition Temperatures of PBS and PBS/OMt Nanocomposites

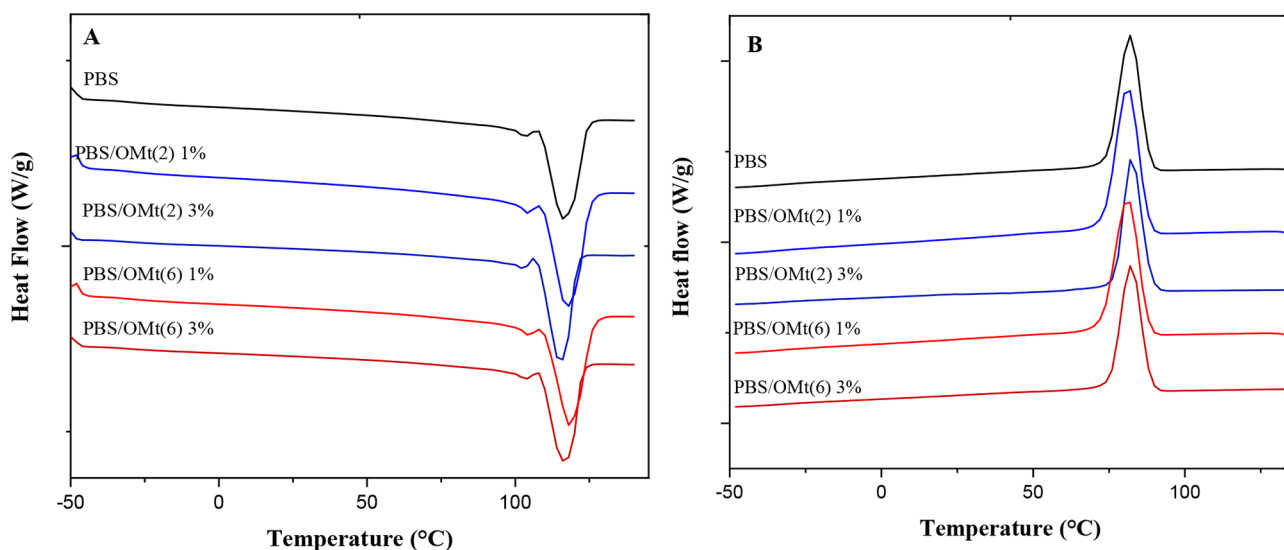| hybrids | decomposition temperature (°C) | | | | | | char residue at 700 °C(wt %) |
	$T_{5\%}$	$T_{10\%}$	$T_{25\%}$	$T_{50\%}$	$T_{75\%}$	T_{max}	
PBS	355	368	385	401	413	408	0.46
PBS/OMt (2) 1%	347	364	380	394	406	402	1.54
PBS/OMt (2) 3%	352	367	384	400	412	408	4.71
PBS/OMt (6) 1%	349	363	380	395	407	403	1.62
PBS/OMt (6) 3%	352	366	383	400	413	408	3.10

Figure 6. DSC curves of PBS and PBS/OMt nanocomposites from (a) heating and (b) cooling second cycles.

The addition of 1% of organoclays led to a reduction of the decomposition temperatures and T_{max} of PBS/OMt (n) 1% nanocomposites by almost 4 to 8 °C. This reduction is ascribed to the premature decomposition of the gemini surfactant molecules present in organoclays, which occurs at lower temperature, hence accelerating the thermal degradation of PBS and promoting the formation of a char layer. The clay particles may also catalyze the thermal degradation rate by accumulating the external heat and acting as a supplementary local heat source.

The decomposition temperatures of nanocomposites prepared with 3% clay loading remained almost unchanged regardless of the organoclay nature. This behavior reflects the good dispersion of the nanofiller within the PBS matrix even for PBS/OMt (6) intercalated hybrids. Similar behavior was reported by several research groups and was related to the low amount of nanoclay in the polymer matrix that cannot significantly affect the hybrids thermal stability.[24]

The residual weight of PBS and related hybrids at 700 °C are presented in Table 1.The high char yields of the nanocomposites compared to PBS are related to the inorganic part in the PBS matrix. The char residue are all the more important as the quantity of OMt increases indicating the positive contribution of organoclays in the formation of a more

Table 2. DSC Data of PBS/OMt Nanocomposites

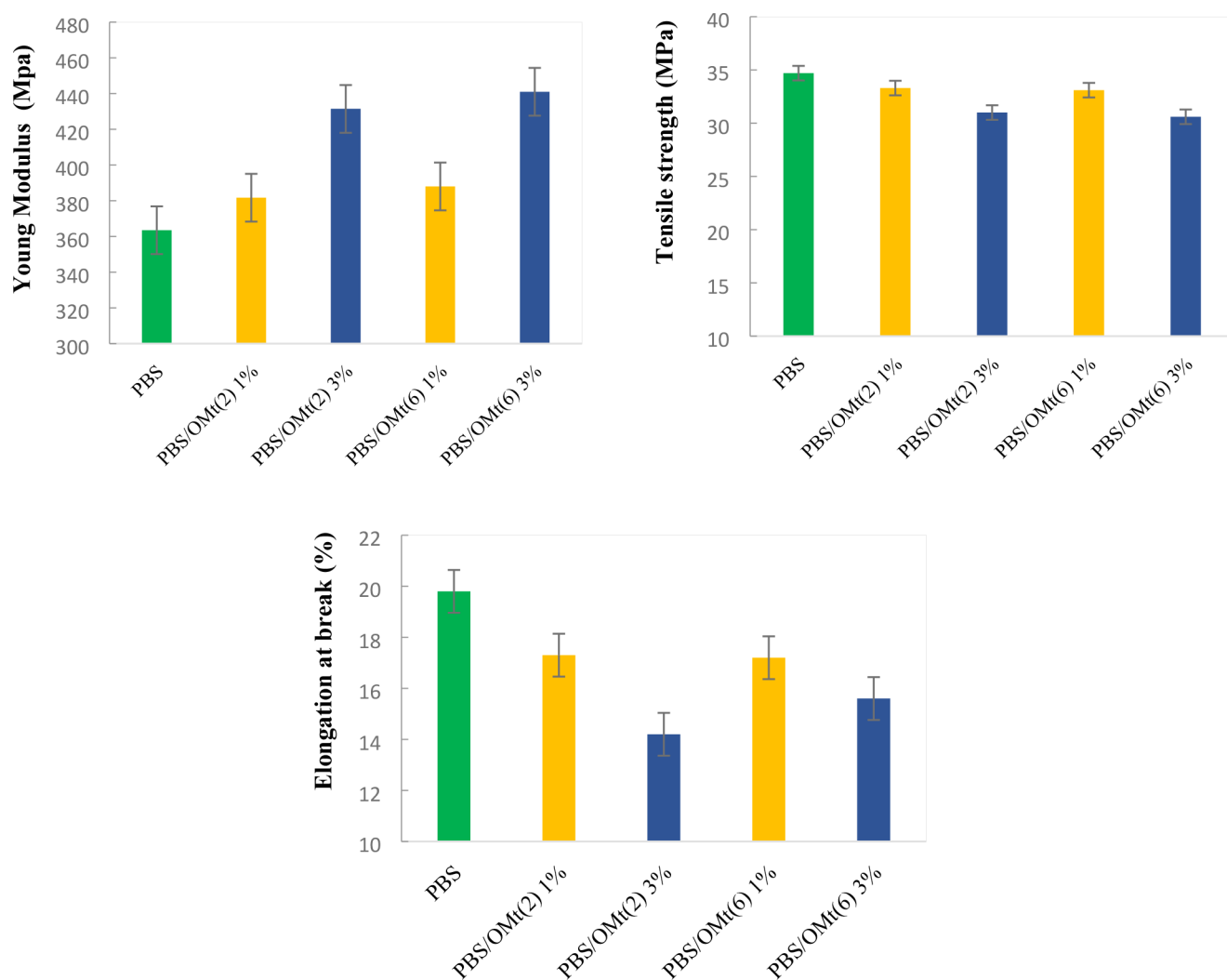| samples	T_{m1} (°C)	T_{m2} (°C)	ΔH_m (J/g)	T_c (°C)	ΔH_c (J/g)	χ_c (%)
PBS	103.17	116.17	−56.61	83.83	56.12	50.87
PBS/OMt (2) 1%	104.17	117.50	−50.56	81.17	50.49	46.24
PBS/OMt (2) 3%	102.67	115	−55.09	82.50	54.63	51.06
PBS/OMt (6) 1%	104.33	118.00	−48.62	81.17	48.58	44.50
PBS/OMt (6) 3%	103.50	116.50	−53.05	82.33	53.72	50.20

Figure 7. Tensile properties of PBS and PBS/OMt nanocomposites.

efficient char.[25] Several studies have reported the contribution of the clay's Bronsted and Lewis acid sites and the strongly protonic catalytic sites resulting from the decomposition of OMt in the enhancement of char formation of polymers.[25,26] The accumulated carbonaceous silicate char at the surface of polymer can acts as a protective barrier which limits the heat and mass transfer into the material. As consequence, the production of combustible gases is usually hampered and the pyrolysis reaction becomes less exothermic.[14] Such features are important for flame retardation applications.

2.6. Differential Scanning Calorimetry. DSC thermograms of PBS and PBS/OMt nanocomposites with different organoclay structure and content, collected from the second heating and cooling scans, are represented in Figure 6. The measured thermal parameters, such as melting temperature (T_m), crystallization temperature (T_c), melting enthalpy

(ΔH_m), crystallization enthalpy (ΔH_c), and crystallinity degree (χ_c), are presented in Table 2.

Similar curves have been obtained for both of neat PBS and PBS/OMt nanocomposites with two distinct endothermic peaks and one exothermic peak in the heating and cooling cycles, respectively.

The observed endothermic peaks are attributed to the melting of two populations of crystal lamella in polymer matrix (PBS). The first small endothermic peak (T_{m1}) at about 103 °C is related to the melting of the original crystallites formed at the isothermal crystallization temperature, while the second one (T_{m2}) corresponds to the melting of the recrystallized crystals.[27] The absence of an additional peak in nanocomposites curves indicates that the incorporation of nanofillers does not induce the formation of a new PBS crystalline form.

Table 3. Tensile Properties of PBS and PBS/OMt Hybrids

hybrids	organoclays	OMt content (w.t %)	Young's modulus (MPa)	tensile strength (MPa)	elongation at break (%)
PBS	/	-	363.5 ± 8.8	34.7 ± 0.9	19.8 ± 1.9
PBS/OMt (2) 1%	OMt (10−2−10)	1	381.7 ± 9.0	33.3 ± 1.2	17.3 ± 0.8
PBS/OMt (2) 3%	OMt (10−2−10)	3	431.4 ± 10.6	31.0 ± 1.6	14.2 ± 1.1
PBS/OMt (6) 1%	OMt (10−6−10)	1	388.0 ± 6.3	33.1 ± 1	17.2 ± 0.8
PBS/OMt (6) 3%	OMt (10−6−10)	3	441.0 ± 9.5	30.6 ± 0.9	15.6 ± 1.2

Table 4. Water Vapor Permeability of PBS and PBS/OMt Nanocomposites

hybrids	PBS	PBS/OMt(2) 1%	PBS/OMt(2) 3%	PBS/OMt(6) 1%	PBS/OMt(6) 3%
$(WVP) \times 10^{-11}(g/m \cdot s \cdot Pa)$	1.08 ± 0.01	0.93 ± 0.05	0.80 ± 0.03	0.96 ± 0.042	0.83 ± 0.04
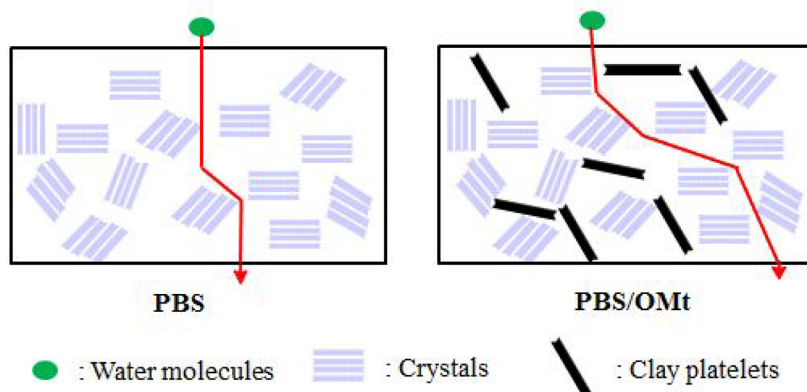
Figure 8. Illustration of the tortuous pathway induced by the incorporation of organoclay nanoplatelets in PBS matrix.

Any significant modification of the melting temperatures (T_{m1}) and (T_{m2}) values was reveled for nanocomposites samples as compared to neat PBS. The temperatures move to slightly higher values from 103 to 104 °C and from 116 to 118 °C, respectively, in the case of nanocomposites reinforced by 1% of OMt. While these temperatures remained constant after the addition of 3% of organoclay.

Similarly, the T_c value was not substantially altered after the addition of nanoclays and decreased by almost 1 to 2 °C for all prepared nanocomposites.

In contrast, the enthalpy of crystallization was significantly decreased particularly for low clay content and for PBS/OMt (6) nanocomposites indicating a reduction in the crystallization rate of PBS. This trend was confirmed by the crystallinity index (χ_c) since low χ_c values were reached by 1% clay-loaded nanocomposites compared to pure PBS while for higher clay loading (3%), the crystallinity index remained almost constant (Table 2).

Generally, the introduction of nanoclays results in the enhancement of the crystallization process due to their role as a heterophase nucleating agent.[5]

In these investigated systems, the nanoclay seems to retard the local lamellar crystallization growth probably by hindering the mobility of the amorphous phase.[15,28] Indeed, the establishment of strong interactions between the functional groups of PBS matrix and the intercalated/adsorbed surfactant molecules in the OMt nanofiller will lead to partial physical immobilization of the polymer chains on the surface of platelets, thus preventing their participation in the flow process and their crystallization. The retarding crystallization effect seems to be dominant for low clay loading reflecting the greater number of interacting sites, while for high clay content,

this behavior will be attenuated by the nucleating effect of the silicate layers which enhance the crystallization rate of PBS.[29]

2.7. Mechanical Properties. The effect of type and amount of organoclays on the tensile properties of nanocomposite films were investigated with respect to the neat PBS matrix. Young's modulus, tensile strength, and elongation at the break parameters extracted from the stress−strain curves (Figure 7) are collected in Table 3. For pristine PBS, a Young modulus of 363.5 MPa was found which is similar to values reported in literature ranging from of 326.3−373.0 MPa.[25,30]

Results showed a significant improvement in Young's modulus with increasing clay content reflecting an improvement in the shiftiness of the hybrids. Young's modulus increased from 363.5 MPa in pure PBS to 381.7 and 388.0 MPa for PBS/OMt (2) 1% and PBS/OMt (6) 1% samples, respectively. These values rise to 431.4−444.0 MPa in hybrids containing 3% organoclays which correspond to an enhancement of 18−21%. The increase of Young modulus is also favored by the lengthening of the gemini surfactant spacer length.

This improvement is mainly due to the high aspect ratio, rigidity, and hardness of clay platelets.[31] An optimal nanodispersion of platelets with considerable Young's modulus of 178−265 GPa[32] in a polymer matrix will enable the enhancement of PBS modulus. Such good dispersion is assured by the establishment of strong interactions between organoclay particles, and the polymer matrix probably through hydrogen bonding between surfactant molecules and PBS as already discussed in the XRD, TEM, and rheology sections.

The impact of organoclay addition on tensile strength values was less pronounced and tends to slightly decrease as the clay content increases regardless of the surfactant structure. This

reduction in tensile strength values could be attributed to the presence of some OMt agglomerates in the blends which can be at the origin of cracks initiation and propagation[30,31,33] as shown in SEM images. Similar behavior has been reported by Tian et al. for PBS/organoclay composites that has been correlated with the surfactant concentration. It has been shown that for surfactant loading higher than 0.6 CEC, a significant decrease of the tensile strength was obtained as result of the aggregation of the excess surfactant molecules which limit the PBS's plastic deformation and PBS—organoclay interactions.[15]

Regarding the ductility of PBS/OMt nanocomposites, a slight decrease of hybrid's elongation at break was noticed with respect to neat PBS and particularly for high organoclay loadings This trend observed in the case of others filled polymer composites[34−36] is mainly attributed to the shrinkage of the cross-section of polymer resisting to deformation due to the addition of nanofillers. The polymer/OMt interface will constitutes a weakness region inducing early break.[37] Others factors can also impact the elongation at the break as the extent of nanofiller dispersion and the orientation of platelets.

2.8. Water Vapor Permeability. Development of biopolymers with improved barrier properties against water vapor permeation is crucial for sustainable packaging applications.

Water vapor permeability (WVP) of the PBS and PBS/OMt films determined from the cup method are presented in Table 4 and Figure 8. It clearly appears that the water vapor barrier properties of PBS-based films are closely dependent on the clay amount and to a lesser extent on the surfactant structure. The WVP of neat PBS film was 1.08×10^{-11} g/m·s·Pa and decreased significantly with the increase of organoclay concentration up to 0.80×10^{-11} g/m·s·Pa for PBS/OMt (2) 3% nanocomposite.

The improvement of the permeation of nanocomposite films by 11−26% with respect to unfilled PBS film is mainly attributed to the tortuous pathway generated by the impermeable clay nanoplatelets for water vapor diffusion (Figure 8). Well-dispersed clay layers lead to an increase in the length of the effective diffusion path and a retardation of the passage of water molecules. This feature becomes more pronounced as the clay content increases as a result of a reduced semipermeable polymer phase volume fraction. Even if exfoliated nanocomposites structures usually exhibit better barrier properties than intercalated homologous due to better degree of dispersion, the morphology of the as-investigated PBS/OMt (intercalated/exfoliated) seems to have little effect on water vapor permeability probably due to the low clay loadings (1−3 wt %). The slightly higher crystallinity of the exfoliated PBS/OMt (2) structure as compared to PBS/OMt (6) homologous reported previously should also participate in the reduction of WVP due to an increase contribution of the impermeable crystalline phase that induces a longer and more complex tortuous path for the water vapor diffusion.

The reduction efficiency in WVP using OMt (10−2−10) organoclay was similar to that reported for nanocomposite films based on PBS and Cloisite 30B prepared by extrusion−calendaring method but with higher organoclay content of 5 wt %.[38] However, this value remains lower than that estimated for PBS/Cloisite 30B nanocomposites obtained by compression-molding process (40%)[38] or PBS/CTAB organomodified beidellite nanocomposites prepared by in situ polycondensation reaction (37%).[5]

The water vapor barrier properties being closely dependent on the method of preparation of the nanocomposite, the molar mass and the crystallinity of the polymer as well as the WVP measurement conditions (humidity, temperature, thickness of the film, etc.), it is difficult to compare these results and draw firm conclusions.

3. CONCLUSION

PBS/organoclay nanocomposites prepared by melt processing method using bivis extrusion were prepared from Na-montmorillonite organomodified with two gemini surfactants bearing different spacer length.

Uniform dispersion of nanofillers into PBS matrix as a result of strong OMt-PBS interactions was confirmed by FT-IR, XRD, SEM, and TEM results. According to the surfactant spacer length, exfoliated structure or mixed intercalated/exfoliated morphology were achieved for PBS/OMt (2) and PBS/OMt (6) hybrids, respectively.

Rheological measurements revealed improved storage modulus, loss modulus (G'') and complex viscosity (η^*) over frequency and clay loading. A pseudosolid-like behavior was obtained for the nanocomposites containing 3 wt % organoclays, which was attributed to the formation of a network of dispersed OMt platelets reflecting the good compatibility between the organomodifers and PBS matrix.

The effect of the organoclay type and concentration on the thermal properties of prepared hybrids was also investigated by TGA and DSC. The nanocomposites were thermally stable at processing conditions and exhibit lower crystallinity as compared to PBS particularly for PLA/OMt (6) with low organoclay content due to restricted molecular polymer chain mobility.

The addition of organoclays increases the hybrid's mechanical properties in term of tensile modulus. Furthermore, substantial enhancement of water vapor barrier properties was achieved for all investigated nanocomposites when compared to neat PBS films with a significant reduction of the water vapor permeability (WVP) by 26%.

These findings could support the benefit of using gemini surfactants based organoclays as nanofillers to prepare biocomposites with improved thermal and mechanical properties for different engineering applications.

4. EXPERIMENTAL SECTION

4.1. Materials. PBS (bionolle#1020) is a commercial product of Showa Denko (Japan) with a weight-average molecular weight (M_w) of 50 000 g/mol. PBS pellets were dried in a vacuum oven at 50 °C for 24 h before melt blending in order to remove residual water.

The clay used in this study is a sodium montmorillonite (Mt) of type Cloisite Na$^+$ (lot 11F14GBX006). It was obtained from Southern Clay Products, Inc., and used without further treatment (CEC = 92.6 mequiv/100 g).

The organoclay (OMt) modifiers were obtained according to the same previously reported ion exchange reaction between sodium montmorillonite (Mt) and gemini surfactants of general formula (4-C$_{10}$H$_{21}$O-Ph-NHCOCH$_2$N$^+$(CH$_3$)$_2$)$_2$(CH$_2$)$_n$, 2Br$^-$ (n = 2 or 6) with 1:1 CEC ratio.[39,40] These surfactants contain 4-decyloxyphenyla-cetamide as a hydrophobic chain and ethylene or hexylene spacer, respectively. The obtained organoclays are denoted as OMt (10−2−10) and OMt (10−6−10), respectively. They

were dried under vacuum and passed through 50 μm sieve before use.

4.2. Nanocomposites Preparation. PBS/OMt hybrids were prepared by simple melt blending method using Thermo Scientific HAAKE Minilab two twin screws extruder. The screw rotation speed was set at 50 rpm at 120 °C in order to achieve the better dispersion of clay particles in the PBS matrix. Two PBS/OMt compositions have been investigated in this study corresponding to 1 and 3 wt % clay content. The PBS quantity was divided into three parts: the first one was premolten at 120 °C; then, the second PBS part premixed with OMt was added. Finally, the last quantity was introduced into the mixture, and the mixing time was maintained for 8 min at 50 rpm. The obtained pellets were hot-pressed at 120 °C into sheets with a thickness of about ±0.25 mm.

The prepared PBS nanocomposites are named hereafter PBS/OMt(n) x%, where n is the number of carbon atoms in the dimeric surfactant spacer length (n = 2, 6) and x represents the clay content in the nanocomposite (x = 1 and 3 wt %).

4.3. Characterization. *4.3.1. X-ray Diffraction.* The X-ray diffraction (XRD) analyses of PBS and PBS/OMt nanocomposites were performed on a XPert Philips X-ray diffractometer at a scanning rate of 0.02 deg/min with Cu K radiation (0.154 nm) at 40 kV and 14 mA. Bragg's diffraction equation has been used to calculate the clay interlayer spacing d_{001} of the different PBS/clay hybrids.

4.3.2. Rheology. Rheological measurements of neat PBS and related nanocomposites were conducted on Anton Paar, CTD 450, Physica MCR 301 rheometer with parallel-plate geometry. Samples (disc diameter = 25 mm, thickness = 1 mm) were dried at 50 °C for 8 h in a vacuum oven before analysis. The limit of the linear viscoelastic region of each sample was previously determined by carrying out a strain sweep at 1 Hz.

The storage modulus (G'), loss modulus (G''), and complex viscosity (η^*) viscoelastic parameters were determined as a function of frequency. The rheometer was operated in the dynamic oscillatory mode at 120 °C, and the frequency sweeps rang was varied from 100 to 0.01 Hz. All measurements were performed under the linear viscoelastic regime with a deformation of 0.5%. Each frequency sweep test was repeated three times using a new specimen.

4.3.3. Scanning and Transmission Electron Microscopies (SEM and TEM). SEM images of PBS/OMt hybrids were obtained from JEOL JSM 6460-LV Microscope. Gold-coated cryo-fractured samples were used for analysis at an accelerating voltage of 10 kV. Nanocomposites morphology was also investigated by TEM by using Hitachi H9000-NAR microscope operating at an accelerating voltage of 100 kV with a resolution of 0.18 nm. Ultrathin sections were obtained at −60 °C with an ultramicrotome (Leica UC7/FC7) equipped with a diamond knife. For each sample, several sections have been sliced and used for TEM observations.

4.3.4. Thermogravimetric Analysis (TGA). Thermogravimetric analysis (TGA) was used to evaluate the decomposition temperatures of the materials. Measurements were undertaken by TGA/DSC1METTLER TOLEDO analyzer from 25 to 800 °C with a heating rate of 20 °C/min under nitrogen. The continuous weight loss and temperature were recorded and analyzed.

4.3.5. Differential Scanning Calorimetry (DSC). Differential scanning calorimetry (DSC) analysis was carried out using a Mettler-Toledo DSC-882 instrument between −50 and 140 °C

under nitrogen atmosphere. From 10 to 15 mg of each sample were sealed in an aluminum crucible and heated from 25 to 140 °C, at a heating rate of 10 °C/min, to eliminate the thermal history of the sample. The sample was held for 2 min at 140 °C then cooled to −50 °C. Finally samples were subjected to a second heating at the same heating rate. The characteristic temperatures and enthalpies were recorded from the second heating and cooling cycle, such as cold crystallization temperature (T_c), melting temperature (T_m), melting enthalpy (ΔH_m), and cold-crystallization enthalpy (ΔH_c).

The degree of crystallinity χ_c (%) was calculated using the equation[41,42]

$$\chi_c(\%) = \frac{\Delta H_c}{\Delta H_m^0(1 - \mu)} \times 100\% \tag{1}$$

where ΔH_m^0 is the theoretical melting enthalpy of 100% crystalline PBS, which is equal to 110.3 J/g[41,42] and μ is the weight fraction of OMt in investigated nanocomposites.

4.3.6. Water Vapor Permeability. The water vapor permeation of PBS and nanocomposites films was evaluated gravimetrically according to the ISO 7783 cups method. The films were previously dried in oven at 50 °C until a constant film weight was obtained then used to seal cylindrical cells filled with 10 g of calcium chloride ($CaCl_2$) desiccant powder. Test cells were placed in a chamber under flowing conditions (25 °C and 48% RH). The water mass uptake of the desiccant powder was monitored as a function of time, and once the steady state was attained, the water vapor transmission rate WVTR ($g·m^{-2}·s^{-2}$) was calculated as the mass of water vapor passing through the film per unit area and time as[43]

$$\text{WVTR} = \frac{W/t}{A} \tag{2}$$

where W is the weight gain of the cups, t is the time (s), and A is the effective area of exposed film (25×10^{-4} m^2). The obtained WVTR values were then used to calculate the water vapor permeability coefficient WVP (g/m·s·Pa) using the equation[44]

$$\text{WVP} = \frac{\text{WVTR} \times d}{\Delta p} \tag{3}$$

where d is the film thickness and Δp is the difference in partial pressure of permeant (water vapor) across the film calculated at T = 23 °C, RH = 50%, and Δp = 1400 Pa.

4.3.7. Tensile Test. Tensile tests of PBS and PBS/OMt films were carried out using Universal MTS type tensile testing machine (Model MTS Synergie RT1000) equipped with a force sensor of 50 N. The tests were performed on dog-bone style film samples. Specimen was clamped between two grips, the crosshead speed was set at 1 mm/s and the initial grip separation was adjusted to 20 mm. All experiences were conducted at temperature of 25 °C and RH = 48%. Young's modulus (E), elongation at break (E), and tensile strength tensile properties of each hybrid were determined from the average values of at least five specimens ± standard error of the mean.

■ ASSOCIATED CONTENT

Ⓢ Supporting Information

The Supporting Information is available free of charge at https://pubs.acs.org/doi/10.1021/acsomega.2c05964.

Plausible interactions between gemini surfactants and PBS matrix, SEM images of prepared nanocomposites under a magnification of 5000, and water vapor permeability (WVP) results of PBS and PBS/OMt nanocomposites (PDF)

■ AUTHOR INFORMATION

Corresponding Author

Salima Saidi-Besbes − *Université Oran 1 Ahmed Ben Bella, Laboratoire de Synthèse Organique Appliquée (LSOA), Département de chimie, Faculté des sciences exactes et appliquées, 31000 Oran, Algeria;* ⓞ orcid.org/0000-0002-7173-6774; Phone: +213 555529020; Email: saidi.salima@univ-oran1.dz, salima_saidi@yahoo.fr

Authors

Khadidja Taleb − *Université Oran 1 Ahmed Ben Bella, Laboratoire de Synthèse Organique Appliquée (LSOA), Département de chimie, Faculté des sciences exactes et appliquées and Faculté de Médecine, 31000 Oran, Algeria*

Isabelle Pillin − *IRDL-FRE CNRS 3744, Université de Bretagne Sud, Lorient 56100, France*

Yves Grohens − *IRDL-FRE CNRS 3744, Université de Bretagne Sud, Lorient 56100, France*

Complete contact information is available at:
https://pubs.acs.org/10.1021/acsomega.2c05964

Author Contributions

Khadidja Taleb: Investigation, Visualization, methodology, Writing - original draft. Salima Saidi-Besbes: Conceptualization, Supervision, Funding acquisition, Writing - review and editing. Isabelle Pillin: Ressources, Yves Grohens: Ressources, Funding acquisition.

Notes

The authors declare no competing financial interest.

■ ACKNOWLEDGMENTS

■ REFERENCES

(1) França, D. C.; Almeida, T. G.; Abels, G.; Canedo, E. L.; Carvalho, L. H.; Wellen, R. M. R.; Haag, K.; Koschek, K. Tailoring PBAT/PLA/Babassu films for suitability of agriculture mulch application. *J. Nat. Fibers.* **2019**, *16*, 933−943.

(2) Ge, F.; Wang, X.; Ran, X. Properties of biodegradable poly(butylene succinate) (PBS) composites with carbon black. *Polym. Sci. - Ser. A* **2017**, *59*, 416−424.

(3) Guidotti, G.; Soccio, M.; Posati, T.; Sotgiu, G.; Tiboni, M.; Barbalinardo, M.; Valle, F.; Casettari, L.; Zamboni, R.; Lotti, N.; et al. Regenerated wool keratin-polybutylene succinate nanofibrous mats for drug delivery and cells culture. *Polym. Degrad. Stab.* **2020**, *179*, 109272.

(4) Gowman, A.; Wang, T.; Rodriguez-Uribe, A.; Mohanty, A. K.; Misra, M. Bio-poly(butylene succinate) and Its Composites with Grape Pomace: Mechanical Performance and Thermal Properties. *ACS Omega* **2018**, *3* (11), 15205−15216.

(5) Ilsouk, M.; Raihane, M.; Rhouta, B.; Meri, R. M.; Zicans, J.; Vecstaudža, J.; Lahcini, M. The relationship of structure, thermal and water vapor permeability barrier properties of poly(butylene succinate)/organomodified beidellite clay bionanocomposites prepared by in situ polycondensation. *RSC Adv.* **2020**, *10*, 37314−37326.

(6) Boonprasith, P.; Woottikanokkhan, J.; Nimitsiriwat, N. Mechanical, Thermal, and Barrier Properties of Nanocomposites based on Poly (butylene succinate)/ Thermoplastic Starch Blends Containing Different Types of Clay. *J. Appl. Polym. Sci.* **2013**, *130*, 1114−1123.

(7) Li, Y.; Wang, S.; Wang, Q.; Xing, M. A comparison study on mechanical properties of polymer composites reinforced by carbon nanotubes and graphene sheet. *Compos. Part B Eng.* **2018**, *133*, 35−41.

(8) Valapa, R. B.; Pugazhenthi, G.; Katiyar, V. Effect of graphene content on the properties of poly(lactic acid) nanocomposites. *RSC Adv.* **2015**, *5*, 28410−28423.

(9) Kováčová, M.; Marković, Z. M.; Humpolíček, P.; Mičušík, M.; Švajdlenková, H.; Kleinová, A.; Danko, M.; Kubát, P.; Vajd'ák, J.; Capáková, Z.; et al. Carbon Quantum Dots Modified Polyurethane Nanocomposite as Effective Photocatalytic and Antibacterial Agents. *ACS Biomater. Sci. Eng.* **2018**, *4*, 3983−3993.

(10) Salimi, M.; Pirouzfar, V.; Kianfar, E. Enhanced gas transport properties in silica nanoparticle filler-polystyrene nanocomposite membranes. *Colloid Polym. Sci.* **2017**, *295*, 215−226.

(11) Nagendra, B.; Mohan, K.; Gowd, E. B. Polypropylene/Layered Double Hydroxide (LDH) Nanocomposites: Influence of LDH Particle Size on the Crystallization Behavior of Polypropylene. *ACS Appl. Mater. Interfaces.* **2015**, *7*, 12399−12410.

(12) Rivas-Rojas, P. C.; Ollier, R. P.; Alvarez, V. A.; Huck-Iriart, C. Enhancing the integration of bentonite clay with polycaprolactone by intercalation with a cationic surfactant: effects on clay orientation and composite tensile properties. *J. Mater. Sci.* **2021**, *56*, 5595−5608.

(13) Fukushima, K.; Tabuani, D.; Camino, G. Poly (lactic acid)/ clay nanocomposites: effect of nature and content of clay on morphology, thermal and thermo-mechanical properties. *Mater. Sci. Eng. C* **2012**, *32*, 1790−1795.

(14) Shih, Y. F.; Wang, T. Y.; Jeng, R. J.; Wu, J. Y.; Teng, C. C. Biodegradable nanocomposites based on poly(butylene succinate)/ organoclay. *J. Polym. Environ.* **2007**, *15*, 151−158.

(15) Tian, Q.; Qi, Y.; Qin, S.; Wu, F.; Long, L.; Xu, G.; Yin, X. Effect of Surfactant Concentration on Thermal and Mechanical Properties of Poly(Butylene Succinate)/Organoclay Composites. *J. Macromol. Sci. Part B Phys.* **2017**, *56*, 474−492.

(16) Karakehya, N. Comparison of the effects of various reinforcements on the mechanical, morphological, thermal and surface properties of poly(butylene succinate). *Int. J. Adhes. Adhes.* **2021**, *110*, 102949.

(17) Taleb, K.; Pillin, I.; Grohens, Y.; Saidi-Besbes, S. Polylactic acid/Gemini surfactant modified clay bio-nanocomposites: Morphological, thermal, mechanical and barrier properties. *Int. J. Biol. Macromol.* **2021**, *177*, 505−516.

(18) Taleb, K.; Saidi-Besbes, S.; Pillin, I.; Grohens, Y. Gemini surfactant based-organomontmorillonites: preparation, characterization and application in pickering emulsion. *J. Dispers. Sci. Technol.* **2022**, *0*, 1−12.

(19) Ni, R.; Huang, Y.; Yao, C. Thermogravimetric analysis of organoclays intercalated with the gemini surfactants. *J. Therm. Anal. Calorim.* **2009**, *96*, 943−947.

(20) Stojšić, J.; Raos, P.; Milinovic, A.; Damjanović, D. A Study of the Flexural Properties of PA12/Clay Nanocomposites. *Polymers* **2022**, *14* (43), 434.

(21) Sinha Ray, S.; Okamoto, K.; Okamoto, M. Structure - Property Relationship in Biodegradable Poly (butylene succinate)/ Layered Silicate Nanocomposites. *Macromolecules* **2003**, *36*, 2355−2367.

(22) Barick, A. K.; Tripathy, D. K. Effect of organically modified layered silicate nanoclay on the dynamic viscoelastic properties of thermoplastic polyurethane nanocomposites. *Appl. Clay Sci.* **2011**, *52*, 312−321.

(23) Murphy, Z.; Kent, M.; Freeman, C.; Landge, S.; Koricho, E. Halloysite nanotubes functionalized with epoxy and thiol organosilane groups to improve fracture toughness in nanocomposites. *SN Appl. Sci.* **2020**, *2*, 2130.

(24) Wu, D.; Wu, L.; Wu, L.; Zhang, M. Rheology and thermal stability of polylactide/clay nanocomposites. *Polym. Degrad. Stab.* **2006**, *91*, 3149−3155.

(25) Wang, Y.; Zhang, S.; Wu, X.; Lu, C.; Cai, Y.; Ma, L.; Shi, G.; Yang, L. Effect of montmorillonite on the flame-resistant and mechanical properties of intumescent flame-retardant poly(butylene succinate) composites. *J. Therm. Anal. Calorim.* **2017**, *128*, 1417−1427.

(26) Laoutid, F.; Bonnaud, L.; Alexandre, M.; Lopez-Cuesta, J. M.; Dubois, P. New prospects in flame retardant polymer materials: From fundamentals to nanocomposites. *Mater. Sci. Eng. R Reports* **2009**, *63* (3), 100−125.

(27) Phua, Y.J.; Chow, W.S.; Mohd Ishak, Z.A. Organomodification of Montmorillonite and Its Effects on the Properties of Poly(butylene succinate) Nanocomposites. *Polym. Eng. Sci.* **2013**, *53*, 1947.

(28) Fu, B. X.; Yang, L.; Somani, R. H.; Zong, S. X.; Hsiao, B. S.; Phillips, S.; Blanski, R.; Ruth, P. Crystallization studies of isotactic polypropylene containing nanostructured polyhedral oligomeric silsesquioxane molecules under quiescent and shear conditions. *J. Polym. Sci., Part B: Polym. Phys.* **2001**, *39*, 2727−2739.

(29) Di, Y.; Iannace, S.; Di Maio, E.; Nicolais, L. Poly(lactic acid)/organoclay nanocomposites: Thermal, rheological properties and foam processing. *J. Polym. Sci., Part B: Polym. Phys.* **2005**, *43*, 689−698.

(30) Chen, G. X.; Kim, E. S.; Yoon, J. S. Poly(butylene succinate)/twice functionalized organoclay nanocomposites: Preparation, characterization, and properties. *J. Appl. Polym. Sci.* **2005**, *98*, 1727−1732.

(31) Chieng, B. W.; Ibrahim, N. A.; Wan Yunus, W. M. Z. Effect of organo-modified montmorillonite on poly (butylene succinate)/ poly (butylene adipate-co-terephthalate) nanocomposites. *Express Polym. Lett.* **2010**, *4*, 404−414.

(32) Chen, B.; Evans, J. R. G. Elastic moduli of clay platelets. *Scr. Mater.* **2006**, *54*, 1581−1585.

(33) Phua, Y. J.; Chow, W. S.; Mohd Ishak, Z. A. Poly(butylene succinate)/ organo-montmorillonite nanocomposites: Effects of the organoclay content on mechanical, thermal, and moisture absorption properties. *J. Thermoplast. Compos. Mater.* **2011**, *24*, 133−151.

(34) Guo, Y.; Yang, K.; Zuo, X.; Xue, Y.; Marmorat, C.; Liu, Y.; et al. Effects of Clay Platelets and Natural Nanotubes on Mechanical Properties and Gas Permeability of Poly (lactic acid) Nanocomposites. *Polymer* **2016**, *83*, 246−259.

(35) Ludueña, L. N.; Kenny, J. M.; Vázquez, A.; Alvarez, V. A. Effect of clay organic modifier on the final performance of PCL/clay nanocomposites. *Mater. Sci. Eng. A* **2011**, *529*, 215−223.

(36) Chang, J. H.; Jang, T. G.; Ihn, K. J.; Lee, W. K.; Sur, G. S. Poly(vinyl alcohol) Nanocomposites with Different Clays: Pristine Clays and Organoclays. *J. Appl. Polym. Sci.* **2003**, *90*, 3208−3214.

(37) Das, A. K.; Suin, S.; Shrivastava, N. K.; Maiti, S.; Mishra, J. K.; Khatua, B. B. Effect of Nanoclay on the Morphology and Properties of Acrylonitrile Butadiene Styrene Toughened Polyoxymethylene (POM)/ Clay Nanocomposites. *Polym. Compos.* **2014**, *35*, 273−282.

(38) Charlon, S.; Marais, S.; Dargent, E.; Soulestin, J.; Sclavons, M.; Follain, N. Structure−barrier property relationship of biodegradable poly(butylene succinate) and poly[(butylene succinate)-co-(butylene adipate)] nanocomposites: influence of the rigid amorphous fraction. *Phys. Chem. Chem. Phys.* **2015**, *17*, 29918−29934.

(39) Taleb, K.; Mohamed-benkada, M.; Benhamed, N.; Saidi-besbes, S.; Grohens, Y.; Derdour, A. Benzene ring containing cationic gemini surfactants: Synthesis, surface properties and antibacterial activity. *J. Mol. Liq.* **2017**, *241*, 81−90.

(40) Taleb, K.; Pillin, I.; Grohens, Y.; Saidi-Besbes, S. Gemini surfactant modified clays: Effect of surfactant loading and spacer length. *Appl. Clay Sci.* **2018**, *161*, 48−56.

(41) Phua, Y. J.; Lau, N. S.; Sudesh, K.; Chow, W. S.; Mohd Ishak, Z. A. Biodegradability studies of poly(butylene succinate)/organo-montmorillonite nanocomposites under controlled compost soil conditions: Effects of clay loading and compatibiliser. *Polym. Degrad. Stab.* **2012**, *97*, 1345−1354.

(42) Tan, L.-c.; He, Y.; Qu, J.-p. Structure and properties of Polylactide/Poly(butylene succinate)/Organically Modified Montmorillonite nanocomposites with high-efficiency intercalation and exfoliation effect manufactured via volume pulsating elongation flow. *Polymer* **2019**, *180*, 121656.

(43) Karkhanis, S. S.; Stark, N. M.; Sabo, R. C.; Matuana, L. M. Water vapor and oxygen barrier properties of extrusion-blown poly(lactic acid)/cellulose nanocrystals nanocomposite films. *Compos. Part A Appl. Sci. Manuf.* **2018**, *114*, 204−211.

(44) Swaroop, C.; Shukla, M. Development of blown polylactic acid-MgO nanocomposite films for food packaging. *Compos. Part A Appl. Sci. Manuf.* **2019**, *124*, 105482.